AIMS Materials Science, 11(1): 173–199.
DOI: 10.3934/matersci.2024010
Received: 08 September 2023
Revised: 12 December 2023
Accepted: 15 January 2024
Published: 05 February 2024

http://www.aimspress.com/journal/Materials

Research article

Silver nanoclusters stabilized with PVP-BSA conjugate: Optical properties approach

Nataly Arrieta-Sandoval, Juan Francisco Hernández Paz, Imelda Olivas-Armendáriz*, Laura Elizabeth Valencia-Gómez and Claudia Alejandra Rodríguez González

Instituto de Ingeniería y Tecnología, Universidad Autónoma de Ciudad Juárez, 450 Del Charro Av., 32310, Ciudad Juárez, Chihuahua, México

* **Correspondence:** Email: iolivas@uacj.mx.

Abstract: The objective of this research was to synthesize fluorescent silver nanoclusters (NC Ag-BSA/PVP) using polyvinylpyrrolidone polymer (PVP) as a stabilizer in conjunction with bovine serum albumin protein (BSA). The nanoclusters were prepared using a wet chemistry reduction technique with two distinctive pathways: the addition of PVP after BSA and the addition of PVP after the metal precursor. The optical properties of the materials were studied in samples with different BSA/PVP molar ratios and varying amounts of metal/reductant. The impact of protein and polymer amounts on fluorescence was determined. The materials were characterized using X-ray diffraction (XRD), infrared spectroscopy (FTIR), thermogravimetric analysis (TGA), X-ray energy dispersive spectroscopy (EDS), dynamic light scattering (DLS), fluorescence spectroscopy, and UV-Vis-NIR spectroscopy.

It was observed that increasing the BSA/PVP ratio resulted in higher fluorescence intensity at λ = 450 nm and a decrease at λ = 600 nm. Regarding the metal/reductant ratio, the amount of metal ions impacted the intensity obtained at λ = 600 nm. The experiments revealed that BSA had the largest effect on fluorescence intensity at λ = 450 nm, with little effect on fluorescence intensity regardless of the amount of polymer used. Due to its one-step synthesis and favorable reaction conditions, the NC Ag-BSA/PVP obtained under the proposed methodology holds promise as an optical marker material. The use of the stabilizing duo BSA-PVP, as well as the proposed amounts in this research, serves as a precedent for developing new experimental syntheses of colloidal nanoparticles.

Keywords: silver nanoclusters; bovine serum albumin; polyvinylpyrrolidone; full factorial design; fluorescence; optical properties

1. Introduction

The application of nanotechnology in the research and development of diagnostic tools for various pathologies is termed nanodiagnosis [1]. This branch of nanomedicine aims to identify diseases in their earliest stages using nanodevices integrated with biological and nanomaterials, given their comparable size to most biological molecules [2]. Quantum dots have emerged as the most used and promising nanomaterials in this context [3,4].

Quantum dots research began over 30 years ago, with the understanding that the optical and electrical properties of small semiconductor particles largely depend on particle size, driven by the quantum confinement effect of charge carriers in confined spaces [5,6]. This effect results in fluorescence, an optical property characteristic of these nanomaterials, which is not observable in bulk materials [7,8]. Metallic nanoclusters, with a composition different from semiconductors, also exhibit fluorescence due to confined free electrons. Achieving quantum confinement in metals requires even smaller particle sizes, creating a gap in the internal energy levels [9]. Metals such as Au, Pt, Cu and Ag are commonly used in nanocluster synthesis [9–12].

The chemical reduction method is widely used for obtaining nanoclusters, where a metal precursor dissociates into a solvent and the metal is reduced. Passivation is crucial for controlled aggregation and containment of nanoclusters. The polyol method, employing a liquid polyol (e.g., ethylene glycol) as both solvent and reducer and incorporating a polymer stabilizer like polyvinylpyrrolidone (PVP), is a common approach [3]. Efforts are being made to develop environmentally friendly synthesis methods, replacing solvents like toluene, trioctylphosphine, and hexane with water [4,13,14]. In water syntheses, sodium borohydride ($NaBH_4$) is often used as a reductant, combined with various stabilizers such as thiolated groups, polymers, and biomolecules like nucleic acids, peptides, and proteins [15–18].

Bovine serum albumin (BSA) has been employed as a stabilizer in the synthesis of semiconductor quantum dots and metallic nanoclusters due to its metal-chelating properties. The thiol groups (-SH) in cysteine residues ionize into reactive anions (-S) under alkaline conditions, allowing coordination with metals like silver. Besides modulating the growth of metal clusters, BSA imparts hydrophilicity to nanoclusters through hydrophilic groups like carboxylate (COO^-) and amino (NH^{3+}), present on the external surface of its globular structure [19].

The first BSA-stabilized nanoclusters were gold nanoclusters, synthesized by Xie et al. in 2009 using sodium borohydride as a reducing agent [18]. This method was later adapted for the synthesis of silver nanoclusters (Agn-BSA) in subsequent research [1,20,21]. In 2011, Mathew et al. synthesized 15 silver atoms clusters (Ag15-BSA) with intense red fluorescence, visible to the naked eye. They incorporated PVP after synthesis to improve particle stabilization, as without the polymer, the metallic clusters tended to fragment within 24 hours [1]. The PVP polymer was introduced to stabilize previously synthesized Ag-BSA nanoclusters. PVP, weakly coordinated with metals through nitrogen and possessing a ketonic group that can interact electrostatically with amino groups in BSA, enhances the electrosteric stabilization of clusters, reducing fragmentation [22,23].

This study proposes incorporating PVP into the synthesis of silver nanoclusters alongside BSA, exploring various polymer addition methodologies. The focus is on investigating the optical properties, including absorbance and fluorescence of the NC Ag-BSA/PVP. Additionally, a full factorial experimental design was employed to evaluate the impact of PVP and BSA concentrations on the optical properties of the NC Ag-BSA/PVP.

2. Experimental methods

2.1. Materials

Silver nitrate ($AgNO_3$ powder, ≥99.0% purity), bovine serum albumin (BSA, lyophilized powder, ≥96.0% purity), sodium borohydride ($NaBH_4$ powder, ≥98.0% purity) and polyvinylpyrrolidone (powder, weight mol. 40,000) were purchased from Sigma-Aldrich. Sodium hydroxide (NaOH, ≥98.9% purity) was purchased from CTR (local supplier). MilliQ water (18 mΩ) served as solvent in the synthesis. Centrifugal filters (Amicon® Ultra-4 100 kDa) were sourced from Merck Millipore.

2.2. Synthesis of NC Ag-BSA/PVP nano-clusters: Experimental design and synthesis methodology

2.2.1. First NC Ag-BSA/PVP experimentation

The initial focus was on obtaining NC Ag-BSA (without polymer). The experiments were based on the methodology developed by Mathew et al. [1], with adjustments made to the reaction conditions based on the stoichiometry described by Elechiguerra, J.L. et al. [2].

Synthesis methodology (samples 1 and 2). Table 1 details the amounts of MilliQ water and BSA used for the synthesis. These were added to a flask, covered with aluminum foil, and the reaction was conducted in the dark at room temperature (25 °C) with low-speed magnetic stirring (60 rpm). The protein was allowed to dissolve for 10 minutes, followed by the addition of 5 mL of an aqueous solution of $AgNO_3$ (10 mM, 8.9 mg) to the prepared BSA solution. The stirring speed was increased to 500 rpm, and after 5 minutes, 0.35 mL of a 1 M NaOH solution (adjusting to pH 12) was added. Immediately afterward, the $NaBH_4$ solution was added dropwise within one minute. The reaction continued for another minute under vigorous magnetic stirring, with the flask covered throughout the reaction. Subsequently, the flask was removed from the stirring and the solution was transferred to a dark vial.

Table 1. Design of Ag-BSA synthesis experiments.

Sample	Amount of water for BSA (mL)	BSA/Solvent ratio (mg/mL)	Ag/BSA molar ratio	1 molar NaOH (mL)	$NaBH_4$/Ag molar ratio
1	5	50	13.9	0.35	0.04
2	5	50	13.9	0.35	0.02
8	28	33	43.6	0	1.62

For colloidal purification, 3.5 mL of the solution was poured into 100 kDa Amicon-Ultra filters and centrifuged for 25 minutes at 4000 rpm. The filtered solution was discarded, and an additional 3.5 mL of water was added to the filter, followed by centrifugation for 15 min at 4000 rpm. Two more washing/centrifugation cycles were performed. The colloidal solution was collected by pipet suction and refrigerated (4–8 °C) in a dark vial. To obtain the powder material, the colloidal solution was lyophilized for 24 hours, and the resulting powder was stored in refrigeration.

Synthesis methodology (sample 8). The synthesis of sample 8 was conducted under room temperature conditions (25 °C) and in the absence of light (Table 1). BSA was introduced into water

and allowed to mix at a low speed for 10 minutes. Silver nitrate powder was then added to 100 mL of water in a beaker, and this mixture was incorporated into the previously prepared water-BSA solution. The resulting blend was stirred for 5 minutes at the maximum stirring speed, with the flask covered by aluminum foil. Subsequently, 2 mL of sodium borohydride solution (18 mg $NaBH_4$/mL) was added, and the reaction was allowed to progress for 1 hour.

Synthesis Methodology (samples 3, 4, 5, 6 and 9). The incorporation of the PVP polymer into the synthesis process for samples 3, 4, 5, 6 and 9 followed the steps outlined in Table 2. MilliQ water and BSA were added to a dark flask at room temperature (25 °C). Under low-speed magnetic stirring, the protein was allowed to dissolve for 10 minutes. An aqueous solution of PVP was prepared and added to the previously prepared BSA solution, mixing for 5 minutes at the maximum stirring speed. Subsequently, an aqueous $AgNO_3$ solution (8.9 mg $AgNO_3$ and 5 mL of water) was incorporated into the BSA-PVP solution. After 5 minutes, 0.35 mL of 1 M NaOH solution was added, followed immediately by the addition of a freshly prepared $NaBH_4$ solution (drop by drop). The reaction was allowed to continue for 5 minutes under vigorous magnetic stirring. Finally, the resulting solution was transferred into a dark vial and stored refrigerated (4–8 °C).

Table 2. Design of Ag-BSA experiments with PVP.

Sample	Amount of water for BSA (mL)	BSA/Solvent ratio (mg/mL)	BSA/PVP molar ratio	Amount of PVP in 2 mL of water	Ag/BSA molar ratio	$NaBH_4$/Ag molar ratio
3	4	33	0.65	121	26.78	0.04
4	4	33	0.65	121	26.78	0.02
5	4	33	0.32	242	26.78	0.02
6	4	50	6.22	24	13.92	0.02
7*	5	50	60.21*	2.5	13.92	0.02
9$^{\Delta}$	5	10	0.60	50$^{\bullet}$	69.62	0.04

* The addition of PVP was after the synthesis.

$^{\Delta}$ The synthesis was carried out in an ice bath.

$^{\bullet}$ PVP was dissolved in 25 mL of water.

Synthesis methodology (sample 7): Sample 7 was prepared following the aforementioned procedure, with the exception of excluding the addition of the PVP solution during the synthesis. Instead, the polymer solution (1 mL of 1.5 mg PVP/mL) was introduced into the reaction solution after 2 minutes of the reaction initiation. This mixture was allowed to continue mixing for an additional 10 minutes.

2.2.2. Optimization of the synthesis of NC Ag-BSA/PVP

To optimize the synthesis of NC Ag-BSA/PVP, two experiments were devised with parameters outlined in Table 3 and Table 4: (1) Varying the BSA/PVP ratio and (2) increasing the amount of solvent used. The synthesis procedure mirrored that of sample 9, serving as a baseline for these optimization experiments.

Table 3. Design of experiment 1, varying the BSA/PVP ratio.

Sample	Amount of water for BSA (mL)	BSA/Solvent ratio (mg/mL)	BSA/PVP molar ratio	Ag/BSA molar ratio	$NaBH_4$/Ag molar ratio
9	5	10	0.6	69.6	0.04
9-1	5	25	1.5	27.8	0.04
9-2	5	50	10	13.9	0.04
9-3	5	50	50	13.9	0.04

Table 4. Design of experiment 2, increasing the amount of solvent in synthesis and amount of reducing agent.

Sample	Amount of water for BSA (mL)	BSA/Solvent ratio (mg/mL)	BSA/PVP molar ratio	Ag/BSA molar ratio	$NaBH_4$/Ag molar ratio
9-4	20	2.5	1.65	69.6	0.04
9-5	20	2.5	1.65	69.6	0.10
9-6	20	2.5	1.65	31.3	0.10
9-7	20	2.5	1.65	31.3	1.00

2.3. Characterization of NC Ag-BSA/PVP

For X-ray diffraction analysis, the lyophilized powder was positioned on a Zero diffraction plate (silicon). Measurements were conducted using a Panalytical diffractometer model X´pert Powder with radiation from a copper filament (k-α of 1.5406 Å). The analysis ran in 0.016 steps, with each step lasting 30 seconds. Chemical analysis employed X-ray energy dispersion spectrometry in STEM transmission mode within a scanning electron microscope (Hitachi equipment model SU5000).

Infrared spectroscopy (FTIR) analysis was performed by Attenuated total reflection of a Germanium crystal (Nicolet 6700). All spectra were recorded using 100 scans and 16 cm^{-1} resolution within the range of 600–4000 cm^{-1}. Thermogravimetric analysis took place in a TA SDT Q600 equipment, using alumina pans with a heating rate of 10 °C/min from room temperature up to 590 °C in air.

Dynamic light scattering (DLS) and zeta potential analyses of the colloidal solution (0.1% by volume of colloidal solution synthetized using MilliQ water like dissolvent) were conducted simultaneously in a Microtrac Nanowave equipment. Absorbance spectra were obtained in a StellarNet spectrometer, silver Nova model, with a deuterium-halogen SL5 light source and optical fibers covering UV-Vis (200–400 nm) and Vis-NIR (400–900 nm) spectra. The samples were 50% dilutions in MilliQ ultrapure water. Fluorescence measurements were taken in liquid samples (50% dilution in MilliQ ultrapure water) using a Shimadzu model RF-5301PC equipment within the range of 400–900 nm.

2.4. Full factorial experimental design 2^2

To assess the impact of PVP and BSA concentration ligands on the optical properties of NC Ag-BSA/PVP, a full factorial design 2^2 (two levels and two factors) was executed. This design comprised 12 experiments (three replicates per sample type), with the first factor being bovine serum albumin protein (mg BSA/mL solvent) and the second factor being the amount of polyvinylpyrrolidone polymer (mg PVP/mL solvent). The output response of the experiment corresponded to fluorescence intensities in two emission regions: 440–460 nm and 580–600 nm. The results are presented in Table 5,

with measurements taken in liquid samples (89% dilution in MilliQ ultrapure water) using the spectrofluorometer technique.

Table 5. Experimental design and output variable (fluorescence intensity in beads).

Standard Order	Run Order	BSA	PVP	Emission Intensity of 450 nm[3]	Emission Intensity of 600 nm[4]
2	1	50	0.5	684.41	885.03
11	2	10	10	105.46	56.38
4	3	50	10	222.45	257.7
3	4	10	10	132.01	47.86
1	5	10	0.5	71.91	100.63
12	6	50	10	256.45	150.79
10	7	50	0.5	677.08	498.66
7	8	10	10	102.8	57.88
6	9	50	0.5	561.2	603.01
8	10	50	10	314.2	486.02
5	11	10	0.5	69.06	95.9
9	12	10	0.5	96.19	148.17

2.5. Analysis of data

The design and data analysis of the experiments was done in the Minitab® program (version 16.0). The deconvolution of spectra was carried out in the Fityk program (version 1.3.1).

3. Results and discussion

3.1. Characterization of optical properties: Absorbance and fluorescence

3.1.1. First NC Ag-BSA/PVP experimentation

In Figure 1, the newly synthesized samples exhibit a darker color, distinguishing them from the samples displayed in Figure 2, which have undergone purification. Figure 2 illustrates that samples 1 and 2, without PVP, were light yellow. Samples 3 and 4 turned light brown, both after purification and one week in the refrigerator in the dark. Samples 5 and 6, after purification and one week in refrigeration, changed to a light-yellow color, with sample 5 acquiring a gel-like consistency. Sample 7 also transformed into a gel, albeit with a light-brown color. Notably, samples 8 and 9 maintained their color, even after a week of refrigeration in the dark.

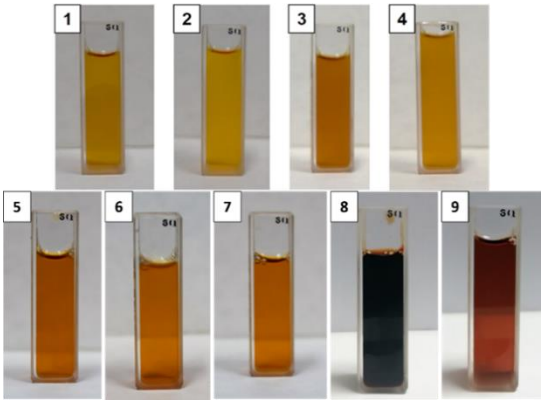

Figure 1. Photographs of the different syntheses (just synthesized and before purification).

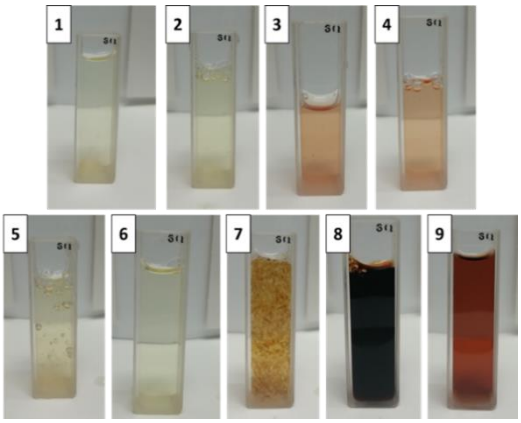

Figure 2. Photographs of the different syntheses (after the purification process and 1 week after being refrigerated in dark containers).

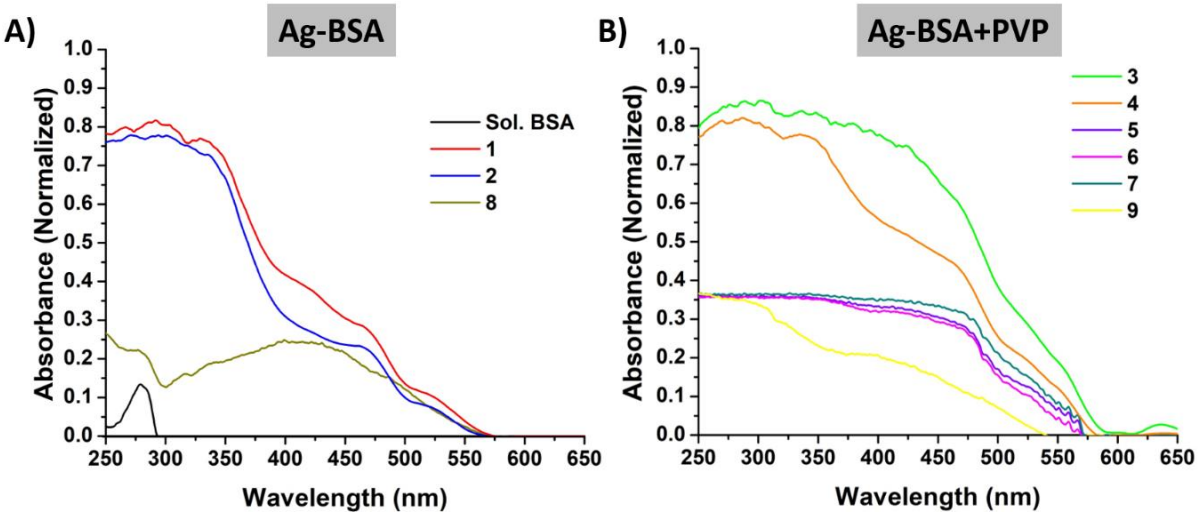

Figure 3. Spectra resulting from UV-Vis absorbance measurements: A) Samples 1, 2 and 8 and B) samples 3, 4, 5, 6, 7 and 9. Obtained 24 hours after the samples were synthesized.

The results from absorbance spectroscopy within the UV-Vis spectral range (200–700 nm) for newly prepared samples (measured 24 hours after synthesis and stored in refrigeration) are presented in Figure 3 and compared to a reference sample (0.1 mg protein/mL water BSA solution).

In Figure 3A, the characteristic absorbance of the BSA protein (black line) is evident around ~280 nm, attributed to the electronic transitions of aromatic groups present in the residues of tryptophan and tyrosine amino acids. Sample 1 (red line) exhibits three small absorption bands at ~528, ~465 and ~417 nm, primarily derived from plasmon resonance (plasmon bands), indicative of the presence of different particle sizes (broad size distribution). Sample 2 shows a disappearance of the band at ~417 nm and an intensification at ~465 nm. Additionally, an initial energy absorption at ~555 nm is observed, suggesting smaller particles in the solution.

This absorbance behavior aligns with findings from Mathew, A. et al., who experimented with different $NaBH_4$ solution amounts and observed that increasing the reducing agent led to the formation of larger nanoparticles [1]. Kim et al. reported that the use of stabilizers like PVP in an ethylene glycol medium as a reducer shifted the initial absorption to longer wavelengths (lower energy), indicating the formation of larger particles [3]. Sample 8 exhibited the highest peak with a broad absorption band at ~415 nm, characteristic of silver nanoparticles with particle sizes greater than ~5 nm [4–7]. Furthermore, an absorbance at ~280 nm due to conjugation with BSA was observed. When compared with the spectrum obtained one week after synthesizing the sample (kept in refrigeration), the same absorption spectrum was maintained (Figure 4A). In contrast, the absorption spectrum of newly synthesized samples 1 and 2 (Figure 3A) displayed a noticeable fading of bands at ~465 and ~417 nm one week after synthesis (Figure 4A and B). A similar behavior was observed in samples 3, 4 and 6. These results are associated with the dissociation or fragmentation of nanoparticles. The broadening and loss of plasmonic absorption signal have been linked to the presence of clusters with particle sizes of ~2 nm [4,8,24]. Desireddy A. et al. found similar decomposition results stabilized with glutathione, observing fragmentation of nanoparticles over 72 hours [25].

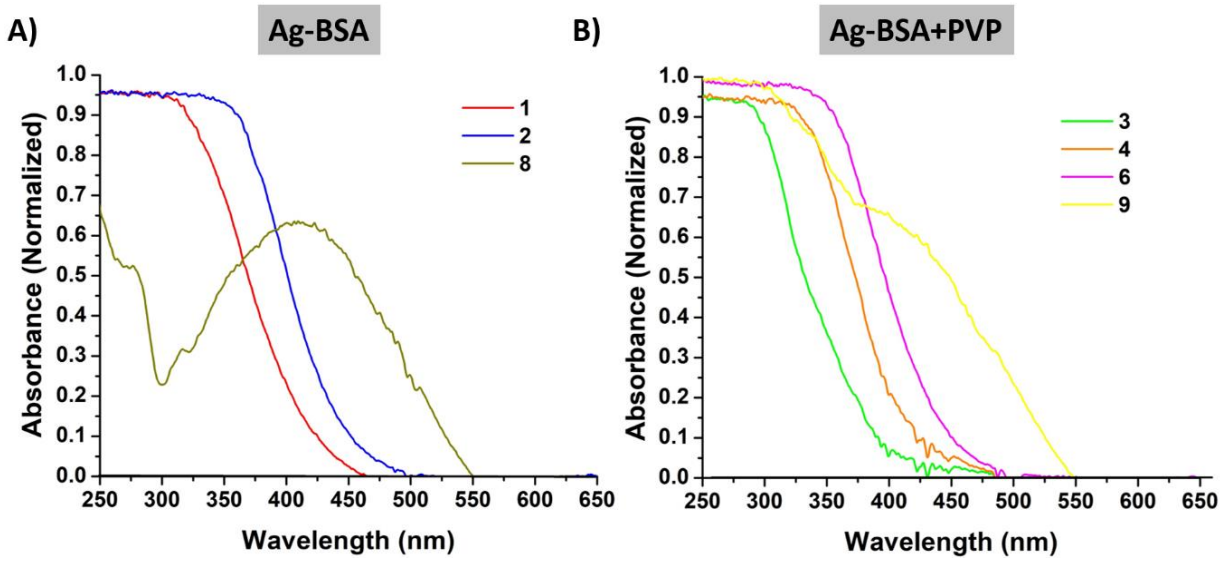

Figure. 4 Spectra resulting from UV-Vis absorbance measurements: A) Samples 1, 2 and 8 and B) samples 3, 4, 5, 6, 7 and 9. Obtained 1 week after samples were synthesized (kept in the dark and refrigerated).

In Figure 4, the absorption spectra of the purified samples stored in refrigeration and darkness are depicted (samples 5 and 7 were excluded from these measurements as they transformed into a gel state after one week of preparation).

In Figure 5, the results of absorbance measurements in the ultraviolet-visible region of sample 9 are presented. The spectrum reveals an absorption edge at ~400 nm, indicative of the plasmonic excitation of the material. After one week in refrigeration and darkness, a slight shift in the initial absorption towards lower energies (longer wavelengths) is observed, with a more pronounced shift for the purified and refrigerated sample. Notably, the absorption edge persists in both samples, albeit with a minor displacement at ~430 nm (refrigerated) and ~440 nm (refrigerated and purified), suggesting potential particle growth.

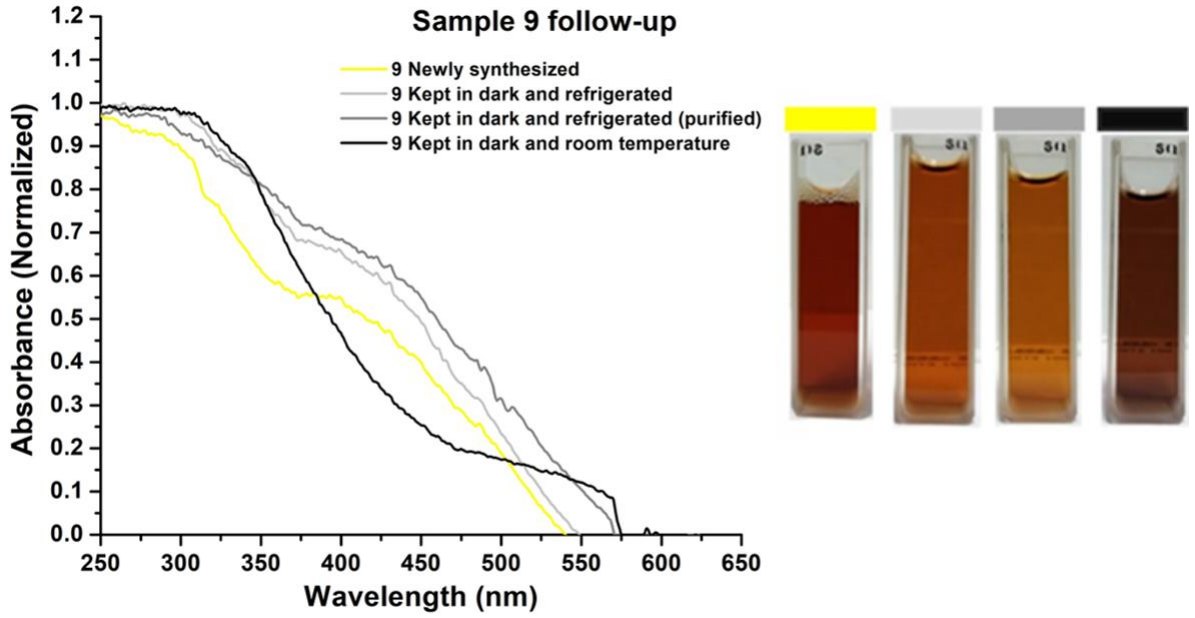

Figure 5. Monitoring the UV-Vis absorbance of the sample 9. Spectrum resulting from the sample one day after the synthesis and kept refrigerated (Newly synthesized). The other samples were analyzed one week after synthesis. On the right side the photographs of the solutions are shown.

For sample 9 stored in the dark at room temperature, the band at 400 nm completely disappears and the initiation of absorption shifts to 600 nm. This is in contrast to samples 1 to 6, where the coloration faded after synthesis. The change in coloration was to an opaque color. DLS results (Figure 6B, sample-9 day 7) indicate an increase of ~86% in the original size (from 7.45 nm to 13.87 nm), and although the size at one week was expected to show absorbance due to plasmon (~400 nm) it was not reflected in the absorbance analysis performed.

In Figure 7, photographs of the unpurified samples stored under refrigeration for one week are presented. The image on the right corresponds to the sample exposed to UV light (365–385 nm). Notably, all samples exhibited fluorescence except for sample 8. The loss of fluorescence in sample 8 can be attributed to the formation of larger particles compared to samples 1–7. The increased particle size in sample 8 is linked to the synthesis stoichiometry, where an intentional saturation of the solution

was pursued by elevating the metal salt and reducer amounts to ensure complete metal reduction. The particle size for sample 8 is determined to be 9.01 ± 2.04 nm (Figure 6A).

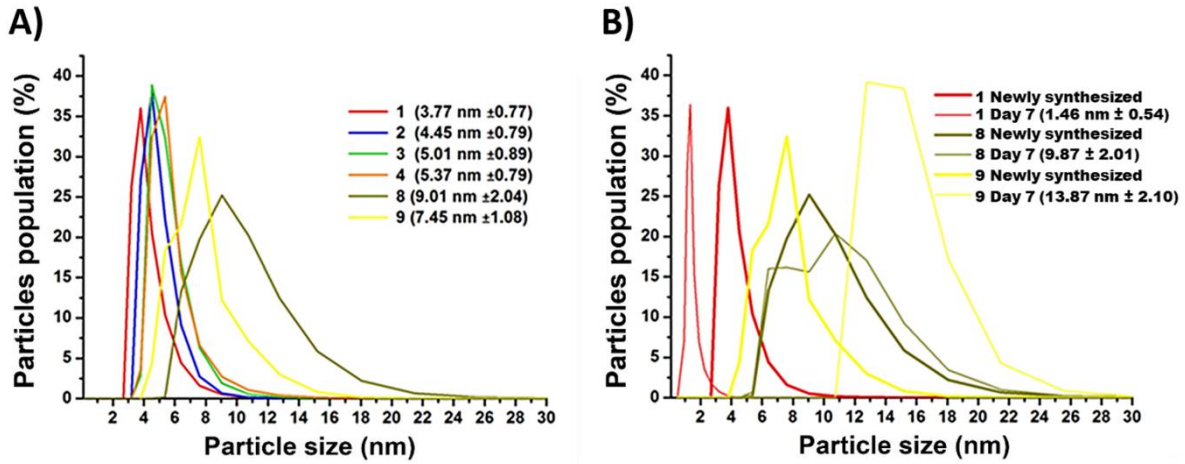

Figure 6. Results of particle size measurements by dynamic light scattering (DLS). A) Samples analyzed 1 day after synthesis and B) results 1 week after keeping the samples in refrigeration and darkness (except sample 9, which was kept at room temperature and darkness for one week). Solutions were prepared 1% by volume of colloidal solution synthetized using MilliQ water.

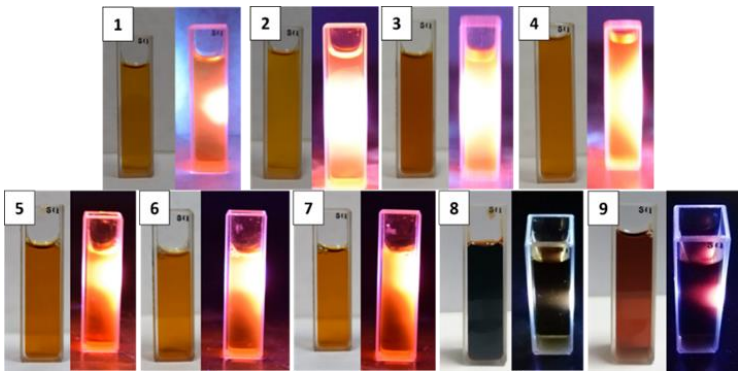

Figure 7. Photographs of the different syntheses (newly synthesized, photographs taken 1 day after synthesis and kept in refrigeration): the photograph under normal light and the corresponding one under UV light (in a dark room) are shown for each sample.

The results of photoluminescence measurements for the newly synthesized samples 1–4 are presented in Figure 8. Notably, the fluorescence exhibits a maximum peak between 600–604 nm, with this light emission associated with the electron decay after transitions between the electronic bands $4d^{10}$ to $4d^{9}5s^{1}$, indicative of the electronic configuration of silver. Borsella et al. attribute the fluorescence at this wavelength (in the orange region of the spectrum) to the presence of Ag_3^{2+} nuclei resulting from the reduction and nucleation of silver ions [26,27]. Additionally, intermediate species (not completely reduced) are attributed to the reducer's amount, with a molar ratio of $NaBH_4$/Ag: 0.04 (observed in samples 1 and 3).

When comparing intensities, sample 2 (without PVP and with half of the reducer) exhibits the highest intensity and a broader emission band than sample 1 (double the amount of reducer). This enhancement could be associated with a higher concentration of particles in the dispersing medium. In contrast, samples 3 and 4 display lower intensity than sample 1. Samples 3 and 4 utilize a molar ratio of BSA/PVP: 0.65, suggesting that the use of PVP minimizes the fluorescence intensity at 600 nm. Furthermore, the BSA/solvent ratio was decreased to 33 for samples 3 and 4, whereas, for samples 1 and 2, it was BSA/solvent: 50.

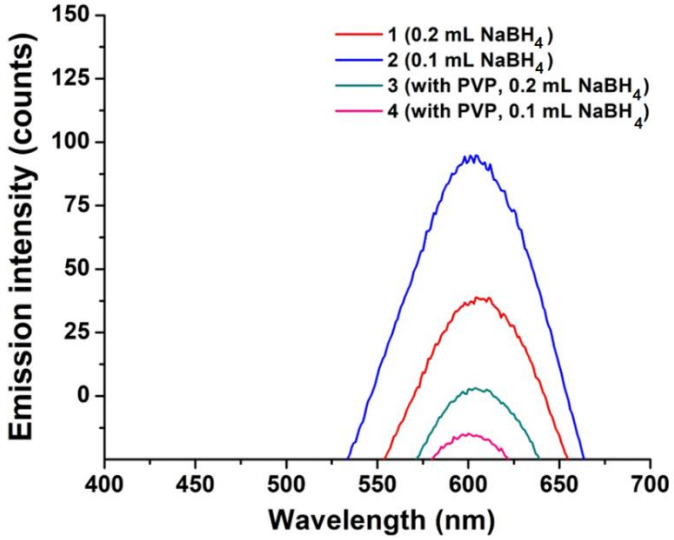

Figure 8. Spectra resulting from fluorescence measurements on newly synthesized samples (with excitation at 365 nm with excitation aperture of 5 nm).

The fluorescence measurements of purified samples refrigerated for one week are presented in Figure 9. The spectra reveal the disappearance of fluorescence at λ = 600 nm, forming bands with a maximum at 450 nm (excited at 365 nm). These findings are consistent with the decomposition or fragmentation of the samples, as previously indicated by absorbance spectroscopy (Figure 4). The fluorescence at 450 nm can be attributed to higher energies, resulting from interactions between pairs of Ag^+ ions [28] with the monomers formed by Ag-BSA.

Comparing the emission intensities at 450 nm between samples 1 and 2 (without PVP) and samples 3 and 4 (with PVP), it is evident that the presence of PVP decreased this signal. This suggests that the interaction between BSA and PVP might partially contribute to the non-dissociation of nanoclusters. Notably, samples 3 and 4 used a molar ratio of BSA/solvent 33, while samples 1 and 2 had a BSA/solvent ratio of 50.

Sample 9, after one week in refrigeration (both purified and unpurified), maintained red fluorescence visible to the naked eye when excited in the range of 365–385 nm (Figure 10). However, it did not exhibit fluorescence when analyzed in a spectrofluorometer, even when testing excitation wavelengths at 5 and 10 nm intervals.

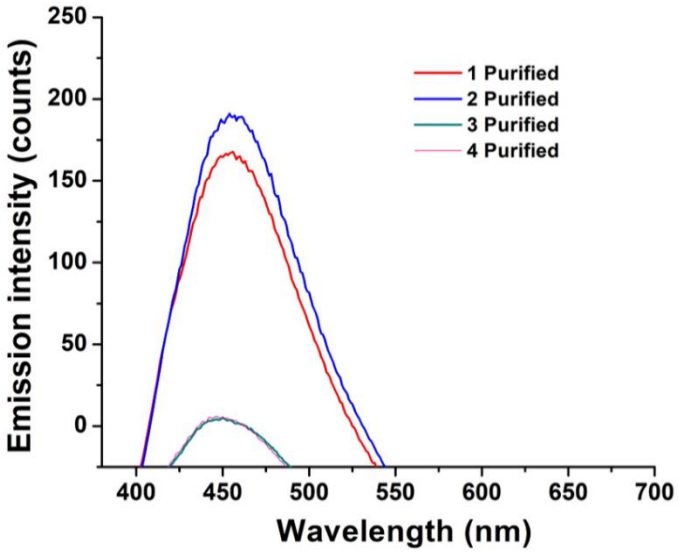

Figure 9. Spectra resulting from the fluorescence measurements of the samples after purification and refrigeration for one week (with excitation at 365 nm with excitation aperture of 5 nm).

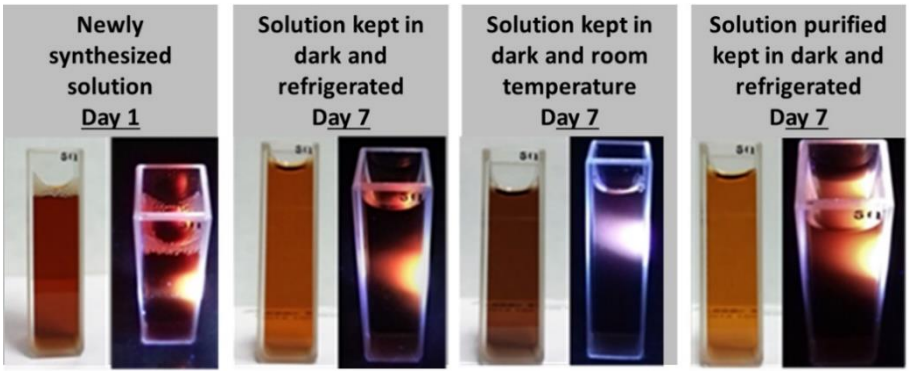

Figure 10. Visual follow-up to sample 9.

3.1.2. Optimization of NC Ag-BSA/PVP

The absorbance of refrigerated samples from the designed experiments 1 and 2 was measured after 24 hours and 1 month of synthesis in liquid samples diluted to 50% in ultrapure water (Figure 11 and Figure 12). In Figure 12A, spectra from the first experiment (varying BSA/PVP molar ratio) indicate that the initiation of energy absorption shifts to lower wavelengths with an increase in BSA amounts. This suggests that the nanoclusters decreased in size due to improved stabilization from protein presence, notably observed in samples 9-2 and 9-3. Compared to sample 9-1 (where the same amount of PVP was used as in sample 9 but 2.5 times more BSA), an increase in stabilization was observed, suggesting smaller particle size. Sample 9-2, using more PVP than 9-3, showed a longer initiation wavelength, indicating larger particle size. Samples 9 and 9-1 exhibited three absorption bands at ~520, ~465 and ~415 nm derived from plasmon resonance, indicative of different particle sizes and broad size distribution. Sample 9-2 showed only two plasmon bands (~465 and ~415 nm) due to higher BSA usage than samples 9 and 9-1. In sample 9-3 (highest BSA/PVP ratio), the

absorption initiation shifted to a shorter wavelength with a small band at ~415 nm. This design suggests that PVP does not provide additional stability to nanoclusters, with BSA being the primary stabilizer. In Figure 12A, dashed lines indicate spectra after 1 month of synthesis. Comparing them with newly synthesized samples, sample 9 maintained the initiation of absorption (~575 nm), although bands at ~520 and ~465 nm decreased in intensity. Sample 9-1 showed decreased intensity in bands at ~465 and ~420 nm, with a shift to higher energies (from 550 to 500 nm), suggesting particle fragmentation or dissociation. Similar results were observed for sample 9-2, where the shift from ~500 to ~430 nm occurred, almost fading the absorption band at 415 nm. Sample 9-3 showed a shift to a shorter wavelength, fading the ~415 nm plasmonic band. This fragmentation phenomenon aligns with results obtained by Desireddy A. et al., indicating particle fragmentation over time [25].

In Figure 12B, spectra from the second experiment (varying solvent and reducer amounts) show that sample 9, with increased solvent and the same reducer amount, exhibited a shorter initiation wavelength, suggesting solvent quantity influences nanocluster size. Comparing sample 9 with others (9-4, 9-5, 9-6 and 9-7) using 4 times more solvent, a shift in the initiation of energy absorption and decreased intensity in ~520 and ~420 nm bands was observed. Sample 9-4, with an increased reducer amount, exhibited a shift after 1 month, indicating potential nanoparticle size increase. Sample 9-5 maintained initiation after 1 month but with decreased ~420 nm band intensity. Comparing samples 9-6 and 9-7, with decreased metal amount, doubled BSA, and varying reducer, sample 9-7 (with more reducer) showed an initiation shift and two absorption bands at ~375 nm and ~285 nm. Both 9-6 and 9-7, after 1 month, displayed initiation shifts at ~390 nm with a small absorption edge at ~350 nm associated with a transition between internal energy levels, possibly involving the excitation of silver electrons [26,27].

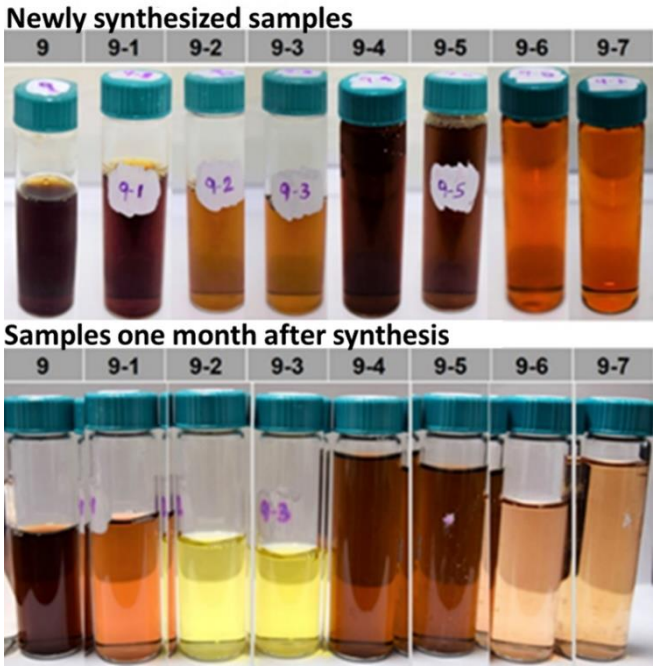

Figure 11. Photographs of the different unpurified samples under normal light.

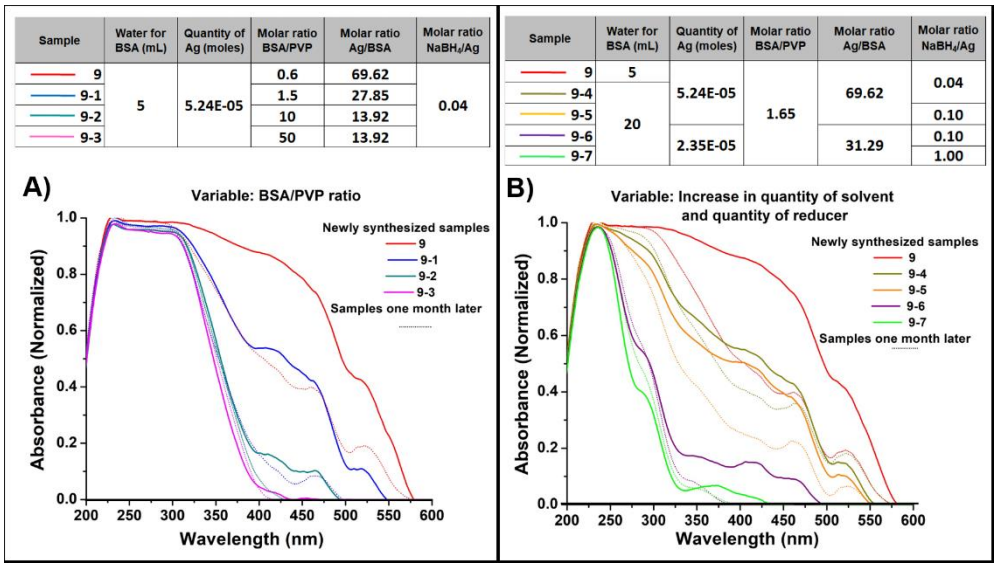

Figure 12. Spectra resulting from UV-Vis absorbance measurements: A) Samples 9, 9-1, 9-2 and 9-3 and B) samples 9, 9-4, 9-5, 9-6 and 9-7. Continuous lines are the newly synthesized samples and dashed lines are those analyzed after 1 month of the synthesis.

Figure 13 displays images of various samples and the corresponding fluorescence spectra in liquid samples in the 400–900 nm emission range (excitation at 370 nm). The freshly synthesized samples exhibit an intense orange color (~590–625 nm) when exposed to UV light (365–375 nm). After one month of refrigeration in the dark, samples 9, 9-1, 9-4, 9-5, 9-6 and 9-7 continue to emit light when exposed to UV light, displaying a red-orange color with decreased intensity in light emission. Notably, samples 9-2 and 9-3, with BSA/PVP molar ratios of 10 and 50, lose the orange fluorescence after 10 days, evident in Figure 13 where a light-yellow color change is observed.

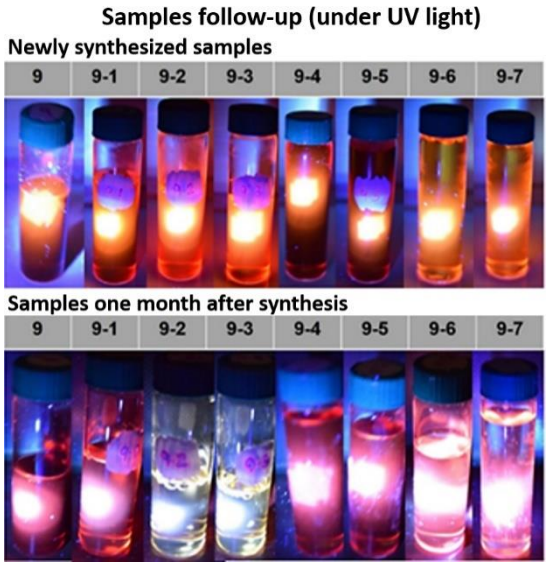

Figure 13. Photographs of the different unpurified samples under UV light ~365–375 nm.

In Figure 14A, the fluorescence spectra of freshly synthesized samples diluted to 50% in distilled water from the first design of the experiment with the variable being the BSA/PVP ratio are presented. Samples 9-1, 9-2 and 9-3 exhibit an emission peak at 600 nm, whereas no response was obtained in sample 9. This absence of response in sample 9 could be attributed to the presence of non-fluorescent species, such as plasmonic nanoparticles larger than 2 nm, which no longer correspond to nanoclusters.

The 600 nm emission is associated with the decay of electrons after transitions between the electronic bands $4d^{10}$ to $4d^{9}5s^{1}$, characteristic of silver's electronic configuration. Borsella et al. attribute this fluorescence at 600 nm (orange region of the spectrum) to the presence of Ag_3^{2+} nuclei derived from the reduction and nucleation of silver ions [26,27]. Additionally, samples 9-1, 9-2 and 9-3 exhibit an emission peak of ~452–456 nm. Sample 9-3, with an emission/excitation aperture of 10.0 nm, displays emission at 455 nm (Figure 15A), and with an aperture of 20.0 nm, a small emission peak is observed at 460 nm for sample 9-1 (Figure 15B).

The increase in the BSA/PVP ratio results in an intensity increase of the peak observed at ~450 nm in the newly synthesized samples, with sample 9-3 presenting the highest emission at 455 nm. This can be attributed to the nucleation of Ag-BSA species, forming larger nuclei due to less stabilization. The emission at ~450 nm is associated with the interactions between pairs of Ag^{+} ions, associated in this synthesis with the monomers formed from Ag-BSA. These results align with Mathew et al., where mixtures of Ag-BSA without a reducer and already reduced metal showed fluorescence at ~445–455 nm [1].

Fluorescence results obtained one month after synthesis for samples 9, 9-1, 9-2 and 9-3 no longer showed the expected signal observed with the naked eye under UV light. Samples 9-1, 9-2 and 9-3 exhibited only the ~450 nm emission peak, suggesting a fragmentation or decay phenomenon. Analyzing the samples with a 20.0 nm emission aperture (Figure 15B) revealed that sample 9-1 exhibited a small emission edge at ~610 nm.

For the second experimental design (increased amount of solvent and reductant), the spectra of the newly synthesized samples diluted to 50% with distilled water (Figure 14B) resulted in an emission at ~590 nm for samples 9-6 and 9-7, with no response from samples 9-4 and 9-5, even when diluted to 16% in distilled water. The results, like sample 9, may be due to the formation of non-fluorescent species (larger particles), potentially related to the amount of metal ions involved. Despite using the same Ag/BSA molar ratio, samples 9-6 and 9-7, with a higher molar ratio, present another small edge at 460 nm, with a more intense signal at ~590 nm and a wider emission peak for sample 9-7, where more reductant was used (10 times more than sample 9-6). This may be associated with a higher concentration of particles in the dispersing medium, generating a broader particle size distribution. Similar to the sample from the first design of experiments, samples 9-6 and 9-7 lost the emission at 590 nm after 1 month of synthesis, and only the signal at 460 nm remained, indicating the fragmentation of the nanoclusters.

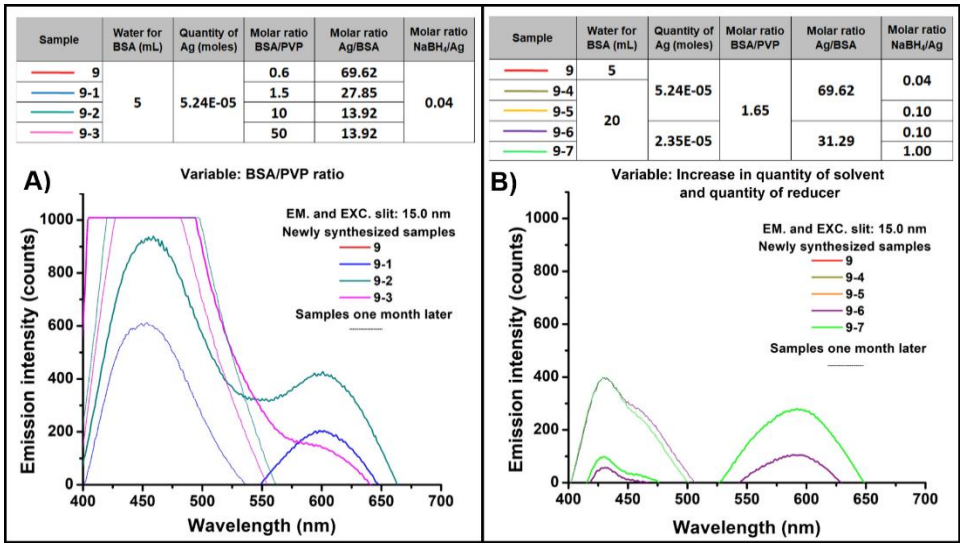

Figure 14. Spectra resulting from measurements of the fluorescence signal: A) Samples 9, 9-1, 9-2 and 9-3 and B) samples 9, 9-4, 9-5, 9-6 and 9-7. Continuous lines correspond to the newly synthesized samples and dashed lines are those analyzed after 1 month of the synthesis (samples kept in refrigeration and darkness), using an emission and excitation aperture or slit of 15.0 nm.

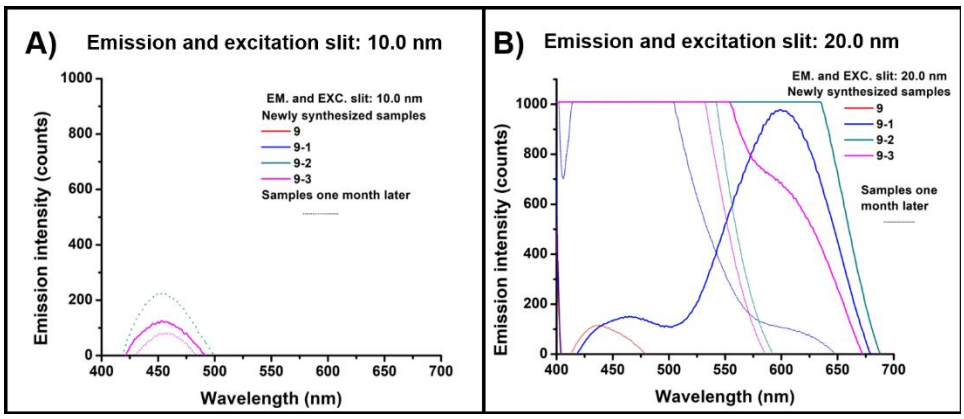

Figure 15. Spectra resulting from measurements of the fluorescence signal of samples 9, 9-1, 9-2 and 9-3. A) Using an emission and excitation aperture or slit of 10.0 nm and B) using an emission and excitation aperture or slit of 20.0 nm. Continuous lines correspond to the newly synthesized samples and dashed lines are those analyzed after 1 month of the synthesis (samples kept in refrigeration and darkness).

Figure 16 illustrates the impact of the BSA/PVP molar ratio on the fluorescence intensity obtained at 450 and 600 nm. The fluorescence intensity, measured with a 15 nm fluorometer shutter, demonstrates a clear dependence on the BSA/PVP molar ratio. In the case of sample 9, which has the lowest BSA/PVP molar ratio, no fluorescence signal is observed at either 450 nm or 600 nm. This absence of fluorescence suggests that the nanoclusters in this sample may not be conducive to emitting light. Moving to sample 9-1, there is no signal at 450 nm, but a noticeable intensity of 600 counts is observed at 600 nm. This indicates that at this BSA/PVP ratio, the sample exhibits fluorescence, albeit

more prominently at 600 nm. Sample 9-2 exhibits a fluorescence signal at 450 nm with an intensity of 928 counts, surpassing the intensity of 414 counts at 600 nm. The increase in the BSA/PVP ratio seems to enhance the fluorescence signal at 450 nm relative to 600 nm. Further elevating the amount of BSA to the maximum, as seen in sample 9-3, follows a similar trend to sample 9-2. This sample shows a higher intensity for 450 nm (1200 counts) compared to the emission at 600 nm, which only registers a fluorescence intensity of 144 counts.

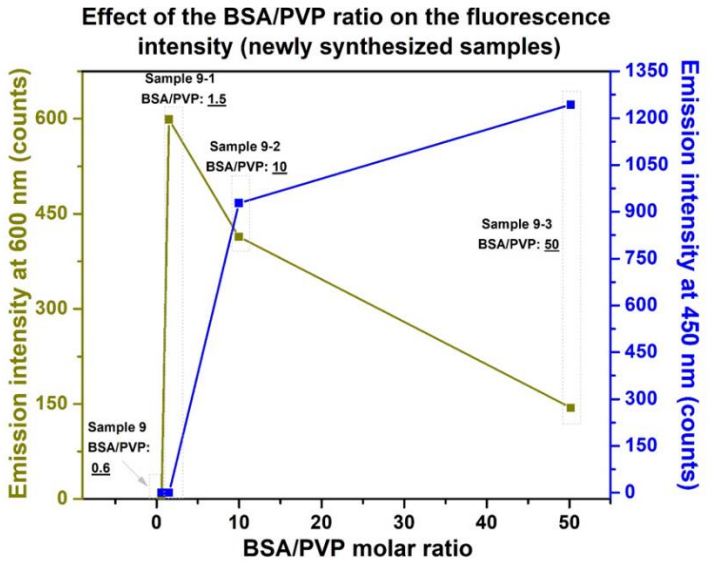

Figure 16. The effect of the BSA/PVP molar ratio on the intensity of fluorescence obtained, at 450 and 600 nm wavelength.

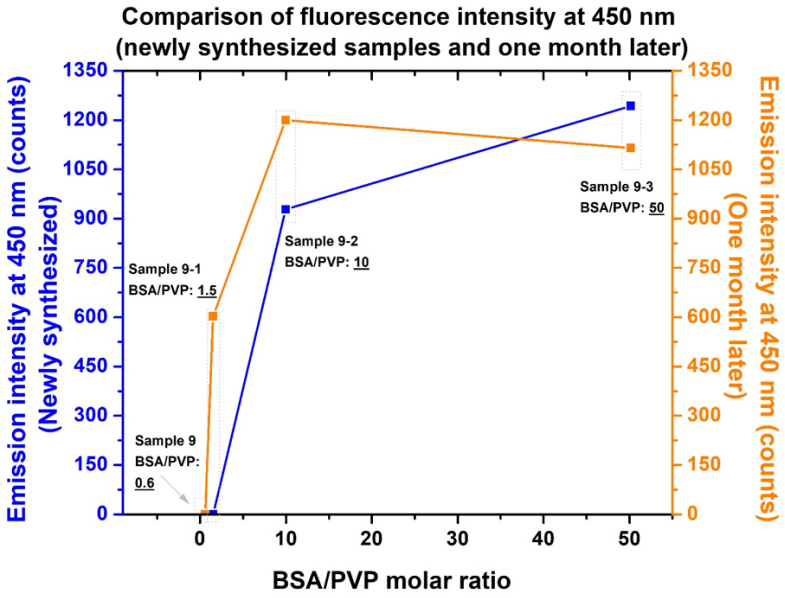

Figure 17. Graph of the effect of the BSA/PVP molar ratio on the intensity of fluorescence obtained at 450 nm, newly synthesized (blue) and the resulting one month after synthesizing it (orange).

Figure 17 compares the intensities obtained from the newly synthesized samples with those after 1 month of synthesis, focusing on the emission at 450 nm. Sample 9 did not exhibit a fluorescence signal, and in sample 9-1, no fluorescence was initially detected at 450 nm, but the intensity increased to 600 counts after one month. Sample 9-2 showed an intensity of 900 (newly synthesized), which increased to 1200 counts one month after synthesis. In contrast, sample 9-3 exhibited a decrease in intensity, with 1244 counts when newly synthesized and 1100 counts after one month.

3.2. Adsorption of BSA protein and PVP polymer on silver nanoclusters

To confirm the presence of both the BSA protein and the PVP polymer adsorbed on the surface of the silver nanoparticles, an infrared spectrum was obtained (Figure 18). The spectrum of the PVP sample revealed characteristic bands at 2951 and 2878 cm^{-1}, corresponding to the asymmetric and symmetric stretching vibrations of the CH bond, respectively. Three absorption peaks at 1400, 1424 and 1500 cm^{-1} were identified as the -N–C- bonds [29]; and at 1286 cm^{-1}, the band was attributed to the stretching vibration of the CN bond [30]. Another observed band at 1669 cm^{-1} indicated the stretching vibration of C=O, while the band at 3438 cm^{-1} was associated with the stretching vibration of -OH present in the hygroscopic PVP sample.

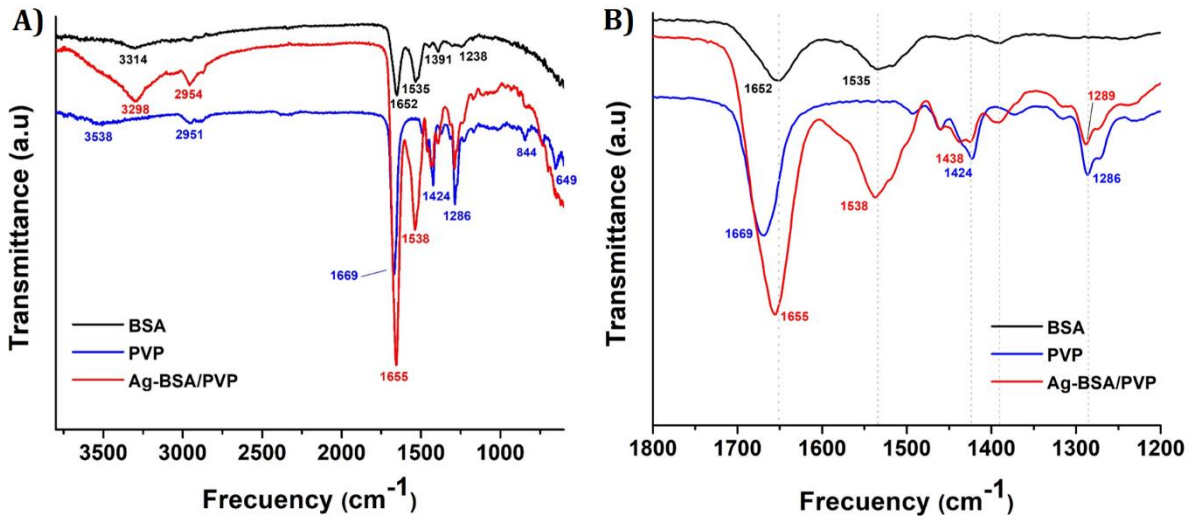

Figure 18. Infrared spectra of the lyophilized sample 9. A) Full spectrum and B) partial spectrum in the region of 1200–1800 cm^{-1}.

The spectrum of the BSA sample exhibited characteristic bands of the protein, including the amide group I at 1652 cm^{-1} (mainly attributed to the stretching vibrations of the C=O bonds and, to a lesser extent, to the CN bond). The band at 1535 cm^{-1}, characteristic of the amide II group, was mainly attributed to the bending of the NH bond and, to a lesser extent, to the stretching vibrations of the C-N and C-C bonds. The broad band at 3314 cm^{-1} was attributed to the stretching vibration of the N-H bond, while the bands at 1238 and 1391 cm^{-1} were attributed to the C-N stretching vibrations present in the amino groups and the O-H bond present in the carboxylic groups in the amino acids, respectively [31,32].

The infrared spectrum of the Ag-BSA/PVP silver nanocluster conjugate (Figure 18, red spectrum) showed the protein and polymer bands with some shifts. One notable shift was observed at a lower

energy for the C=O bond, appearing at 1655 cm^{-1} (compared to 1669 cm^{-1} for PVP alone). This shift may be attributed to the electrostatic interaction between the PVP ketone group and the amino NH groups of BSA [23]. Other shifts were observed, such as the BSA NH stretching vibration from 3314 to 3298 cm^{-1}, the amide II band (NH bending) from 1535 to 1538 cm^{-1}, and the stretching vibration of the CN bond from 1286 to 1289 cm^{-1}. These shifts could be attributed to possible coordination bonds of the PVP nitrogen with the silver atom [22].

To identify the presence of the PVP polymer and the BSA protein, thermogravimetric analysis was conducted. In Figure 19, the thermogram and the first derivative of the mass loss for lyophilized sample 9 (Ag-BSA/PVP) of PVP and BSA are presented. The thermogram (Figure 19A) indicates that the degradation of sample 9 commenced at 230 °C, signaling the mass loss attributed to the BSA content [33,34]. Subsequently, around ~400 °C, another mass loss occurs, corresponding to the initiation of PVP decomposition [35]. Figure 19B, representing the percentage rate of weight loss concerning temperature, displays two inflection points in sample 9. The first (271 °C) aligns with the presence of BSA, while the second (414 °C) corresponds to the PVP polymer adsorbed on the metallic nanoparticles.

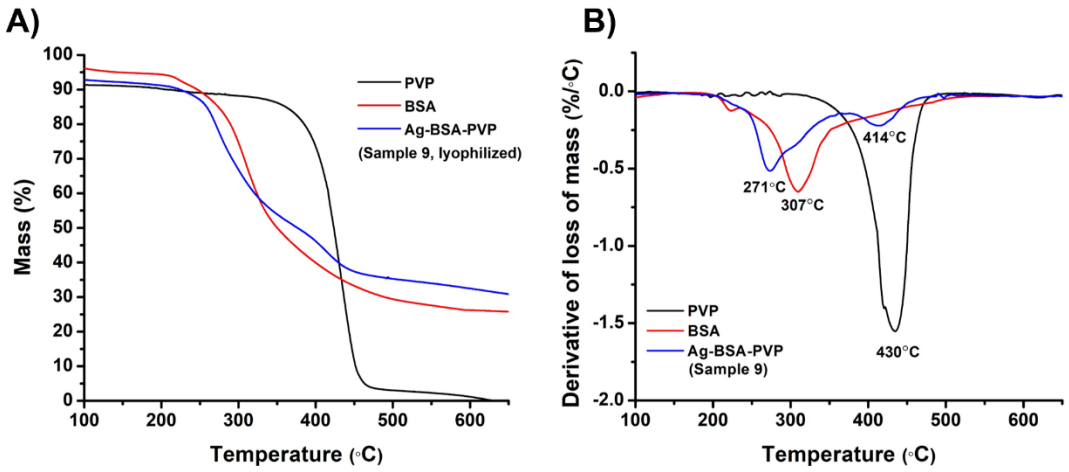

Figure 19. Thermogravimetric analysis. A) Loss of mass and B) first derivative of loss of mass of the lyophilized sample 9, of the PVP, and of the BSA.

3.3. Structural characterization and size of Ag-BSA/PVP nanoclusters

In Figure 20A, the diffractogram from the powdered sample 9-1 is presented, which underwent heat treatment at 500 °C for 2 hours to decompose the adsorbed organic material covering the silver. This treatment promotes the growth of metallic particles, resulting in narrowed characteristic peaks. The identified peaks correspond to the lattice planes (111), (200), (220), (311) and (222), aligning with the FCC phase of silver, as referenced in the JCPDS crystallographic file No. 04-0783.

Chemical analysis using X-ray dispersive energy detector (EDS) (Figure 20B) was performed on sample 9-1 (lyophilized powder). The observed elements include Ag, S, C, O, Na and Al. The presence of S is attributed to cysteine residues in the protein, while C and O are linked to the amino acids constituting the BSA protein and the PVP polymer adsorbed on the particle surface. The existence of Na is associated with sodium borohydride and sodium hydroxide used in the synthesis, and the

presence of Al is attributed to the use of aluminum films to cover the reaction flask during synthesis. The particle size distribution of sample 9-1 was obtained by dynamic light scattering and is shown in Figure 20C, revealing an average size of 11.23 ± 2.17 nm, which represents both the size of the metallic cluster with the BSA layer adsorbed to the nanocluster (also called "protein corona") [36] as well as the polymer electrostatically adsorbed to the BSA.

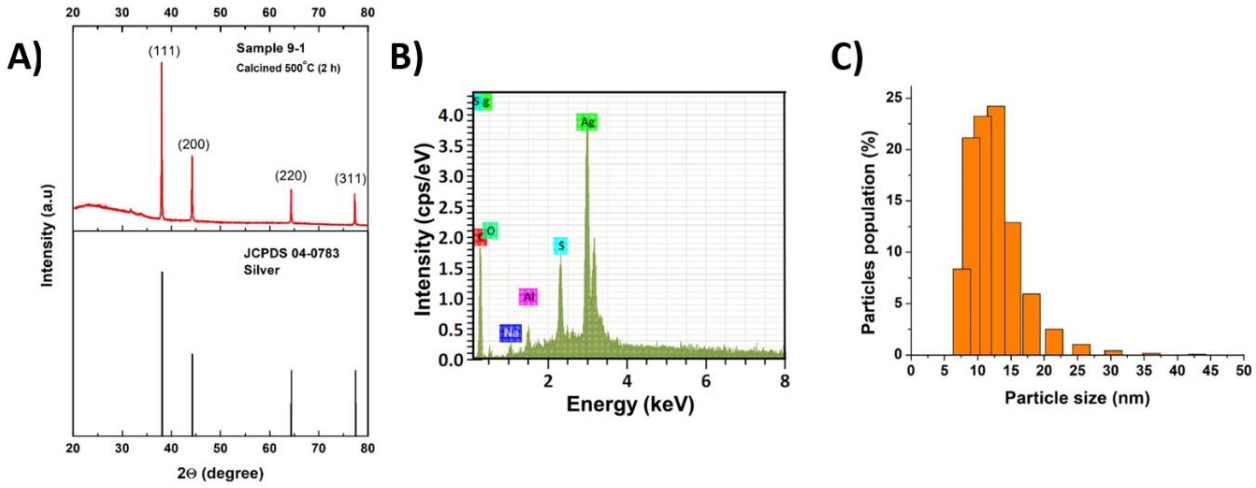

Figure 20. A) X-ray diffraction pattern obtained from powder sample 9-1 calcined at 500 °C for 2 hours (upper), compared with the silver diffraction pattern (JCPDS 04-0783) in lower graph, B) composition analysis of sample 9-1 obtained by X-ray energy dispersion spectrometry and C) particle size distribution of sample 9-1 obtained by dynamic light scattering (0.1% by weight lyophilized powder using MilliQ water).

3.4. Full factorial design 2²: Impact on fluorescence

The absorbance and fluorescence signals obtained for each sample group are illustrated in Figure 21, with each line representing the average of three replicates. In Figure 21A, the emission spectra for each sample group reveal two peaks. The first, with higher energy at 443–457 nm, is attributed to interactions between Ag^+ ion pairs [28], aligning with the monomers formed from Ag-BSA in this synthesis. This finding resonates with Mathew et al., who observed a similar emission in the range of ~445–455 nm in Ag-BSA mixtures without a reducer, as well as in a synthesis solution after metal reduction [1]. The second emission peak falls in the wavelength range of 576–601 nm, associated with the decay of the electron during transitions between the electronic bands $4d^{10}$ to $4d^9 5s^1$, a characteristic of the electronic configuration of silver. Borsella et al. attribute this fluorescence (orange region) to the presence of Ag_3^{2+} nuclei resulting from the reduction and nucleation of silver ions [25,26].

In the emission spectra, the group of samples 1 (black line), utilizing the maximum PVP and minimum BSA, exhibits the lowest intensity in both the 580–600 nm and 440–460 nm ranges. Conversely, the group of sample 3, with the same BSA amount but the minimum PVP (0.5 mg/mL), displayed the lowest intensity in the 440–460 nm range but greater intensity in the 580–600 nm range. The group of samples 2 (red line), using the maximum BSA and minimum PVP, presented the highest intensity in both emission ranges. Additionally, the group of sample 4 (blue line), with the same protein

amount as sample 2 but the maximum PVP, showed a decrease in emission intensity in both ranges compared to the group of samples 2.

Figure 21B displays the absorbance spectra of the samples. An intense absorption edge at 279 nm is observed in the group of sample 2, indicating the characteristic absorbance of the BSA protein due to electronic transitions in aromatic groups present in tryptophan and tyrosine amino acid residues. The increased signal aligns with the fact that the maximum protein value was utilized in this sample. The group of sample 4 exhibited a similar behavior, given the same maximum BSA value. Conversely, samples 1 and 3 showed the lowest intensity at 279 nm, indicating the use of the minimum BSA value.

Comparing the spectra of sample groups 2 and 4, where the maximum protein value was employed, a slight absorption edge at ~346 nm is observed in both spectra, associated with a transition between internal energy levels. In the case of silver, this is linked to the excitation of electrons from the $4d^9 5s^2$ energy level to the $4d^9$ electronic level [25,26]. In sample 2, where the minimum PVP was used, this signal decreased in intensity. Both samples exhibited absorption bands attributed to plasmon resonance (plasmon bands) at ~415 nm and ~465 nm, with lower intensity in sample 2, utilizing the minimum PVP. Sample 4 displayed absorption edges at ~640 and ~673 nm, consistent with previous observations (samples 9-2 and 9-3, Figure 13A). Maintaining a maximum protein level of 50 mg/mL but decreasing the polymer amount, an absorption initiation at shorter wavelengths is observed, indicative of smaller particle size. This trend was not consistently observed in the spectra of the groups of samples 1 and 3. Samples with the minimum BSA value and both minimum and maximum PVP values, respectively, exhibited initiation at longer wavelengths in the group of sample 3, where the minimum polymer amount was used.

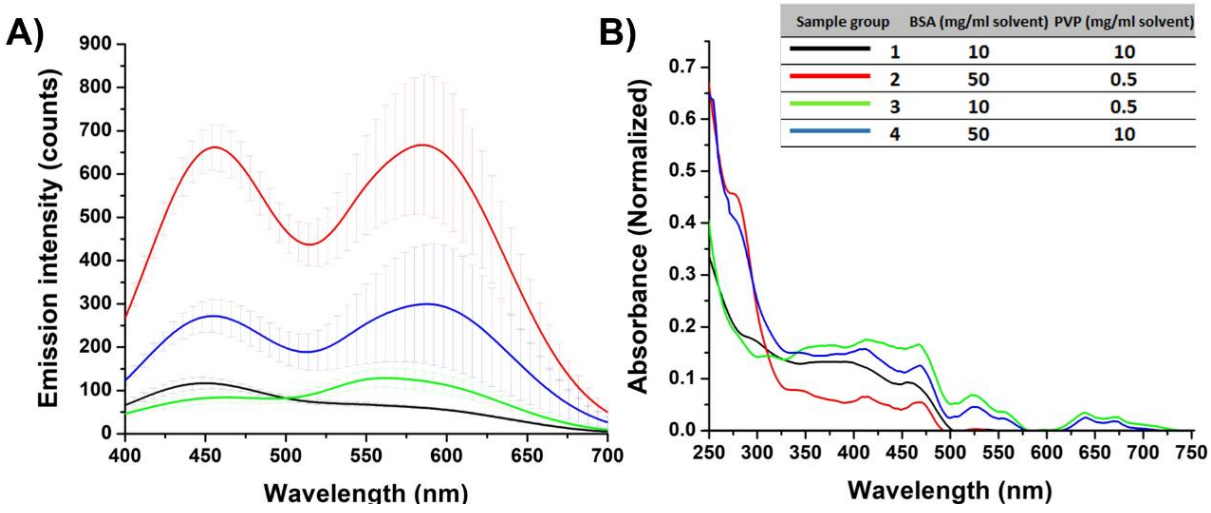

Figure 21. A) Emission spectra presenting the error bar as the standard deviation of the data from three replicates and B) average of the absorbance spectrum from three replicates of each sample.

In Figure 22, the emission spectra of each sample group (three replicates) are depicted, showcasing the outcomes for both maximum and minimum values of the experienced factor. Deconvolution reveals signals at 440–460 nm and 580–600 nm, alongside the signal in the range of 530–550 nm.

Upon comparing these results with the previously obtained data (samples 9, 9-1, 9-2 and 9-3, Figure 14A), a consistent trend is observed concerning the BSA/PVP ratio. Both experiments exhibited an increase in the intensity of the peak around ~450 nm in newly synthesized samples (9-1, 9-2 and 9-3). This phenomenon is notably pronounced in the sample groups of samples 2 and 4, where the maximum protein value of 50 mg/mL was utilized (Figure 22).

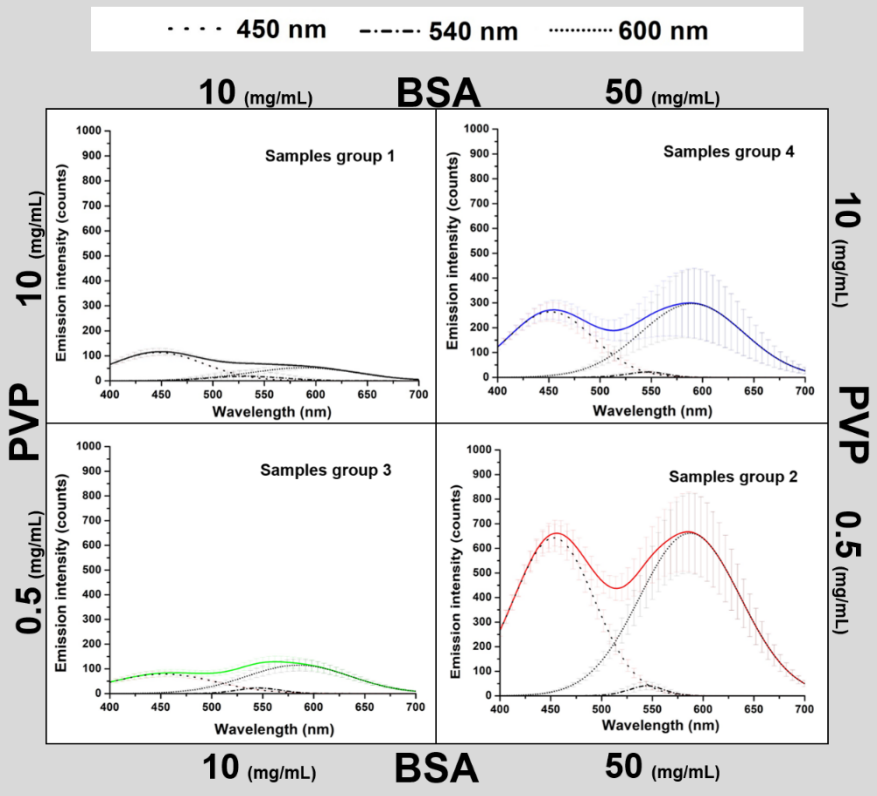

Figure 22. Emission spectra and contributions derived from the deconvolution process. The continuous lines show the average model of the three replicates per sample group, and the dashed lines correspond to the average of three replicates of the signals derived from the deconvolution (signals at 440–450 nm, 530–550 nm and 580–600 nm).

The impact of experimental factors, namely PVP and BSA, on fluorescence intensity within two emission regions (440–460 nm and 580–600 nm) was assessed through an analysis of variance (ANOVA) as outlined in Table 6. The *p*-values (<0.05) derived from the analysis of fluorescence intensity data within the 440–460 nm range indicated that the influence of each factor and their interactions were all statistically significant (p = 0.000). In contrast, the ANOVA results for fluorescence intensity within the 580–600 nm range revealed that the effect of the interaction between BSA and PVP factors is not statistically significant (p = 0.083).

Table 6. Analysis of variance for the two emission intensities studied.

440–460 nm						
Source	GL[a]	SC Sec.[b]	SC adjust.[c]	CM adjust.[d]	*F*[e]	*P*[f]
Main effects	2	468854	468854	234427	126.52	0.0000
BSA	1	381049	381049	381049	205.65	0.0000
PVP	1	87805	87805	87805	47.39	0.0000
2-interactions of No. of factors	1	126629	126629	126629	68.34	0.0000
BSA*PVP	1	126629	126629	126629	68.34	0.0000
Residual error	8	14824	14824	1853		
Pure error	8	14824	14824	1853		
Total	11	610306				
580–600 nm						
Source	GL[a]	SC Sec.[b]	SC adjust.[c]	CM adjust.[d]	*F*[e]	*P*[9]
Main effects	2	605229	605229	302614	17.26	0.001
BSA	1	469807	469807	469807	26.79	0.001
PVP	1	135422	135422	135422	7.72	0.024
2-interactions of No. of factors	1	68951	68951	68951	3.93	0.083
BSA*PVP	1	68951	68951	68951	3.93	0.083
Residual error	8	140274	140274	17534		
Pure error	8	140274	140274	17534		
Total	11	814454				

[a] degrees of freedom

[b] sequential sum of squares

[c] adjusted sum of squares

[d] mean squares adjusted

[e] F test value

[f] *P* value. S = 43.0458 R^2 = 97.57% R^2 (adjusted) = 96.66%

[g] *P* value. S = 132.417 R^2 = 82.78% R^2 (adjusted) = 76.32%

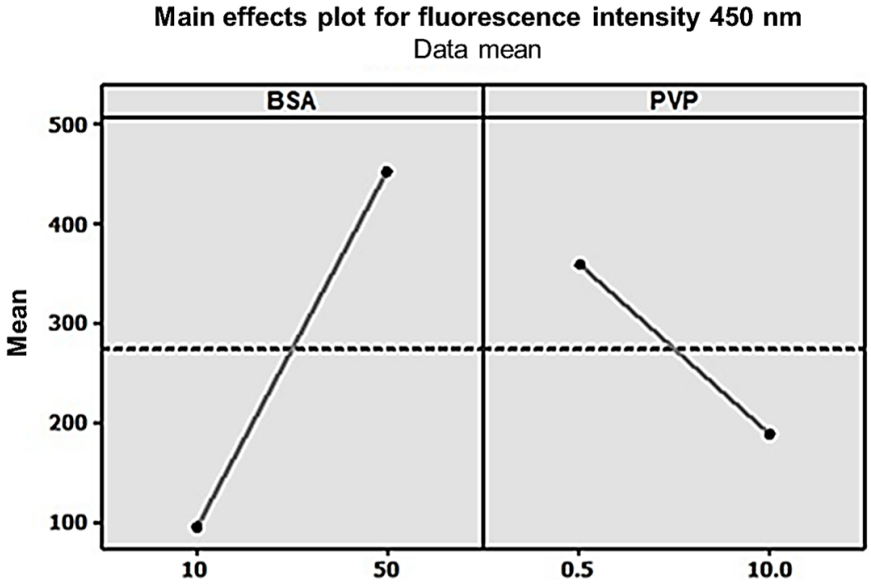

Figure 23. Main effects for the average fluorescence intensity of 440–460 nm. For the BSA factor, the maximum and minimum units correspond to 10 and 50 mg/mL solvent, and PVP factor 0.5 and 10.0 mg/mL solvent.

Figure 23 illustrates the impact of each factor on fluorescence intensity within the 440–460 nm range. It is evident that the highest fluorescence intensities are achieved by increasing the concentration of BSA. Conversely, to enhance fluorescence, PVP concentration should be kept to a minimum.

Given the statistical significance of the BSA and PVP interaction for fluorescence intensity within the 440–460 nm range, a detailed analysis was conducted (Figure 24A). The results demonstrate that higher fluorescence is observed with an elevated concentration of protein and a lower concentration of PVP. Interestingly, when utilizing the minimum level of the BSA factor (depicted by the black line), the impact of PVP on fluorescence intensity is minimal.

In Figure 24B, the Pareto diagram of standardized effects presents the relevance of factors in descending order. BSA emerges as the most influential factor, followed by the BSA/PVP interaction and, finally, PVP. All these factors are statistically significant at the confidence level ($\alpha = 0.05$).

To maximize the signal or enhance fluorescence intensity within the 440–460 nm range, an equation derived from data analysis using Minitab is obtained (Int. Emission = 102 + 8.91 BSA – 18.0 PVP). It is evident that BSA plays a pivotal role in influencing emission intensity.

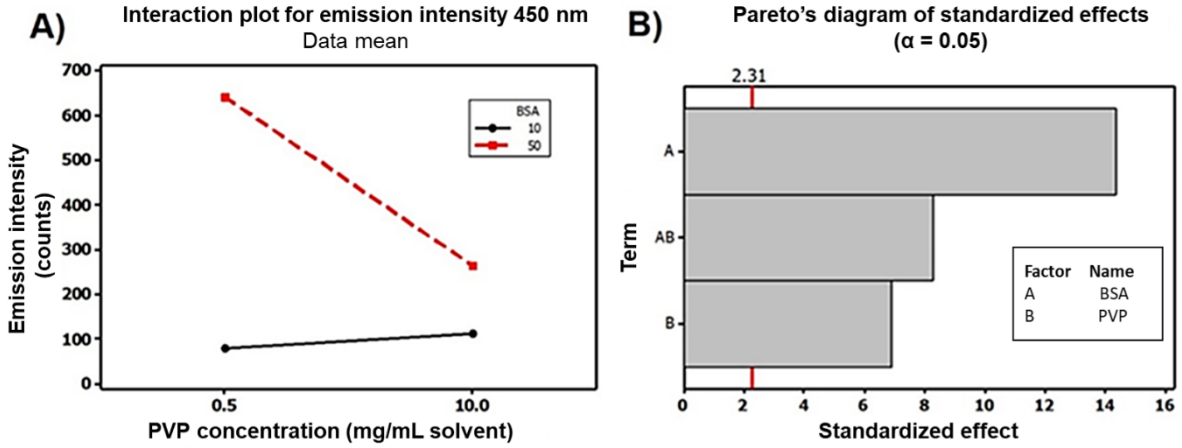

Figure 24. A) Interaction of the BSA and PVP factors for the emission intensity of 450 nm (showing average values of fluorescence intensity) and B) pareto diagram of the standardized effects.

4. Conclusions

Fluorescent silver nanoclusters were successfully obtained by incorporating polyvinylpyrrolidone (PVP) polymer as a stabilizer along with bovine serum albumin (BSA) protein, employing two distinct PVP incorporation methodologies. Visual monitoring over 30 days for the optimized colloids revealed slower fragmentation. Colloids obtained through the first methodology (PVP addition after introducing BSA at room temperature) experienced complete fragmentation within 7 days post-synthesis. However, the introduction of an alkaline environment during the dissolution of lyophilized powder of Ag-BSA/PVP nanoclusters significantly impacted the fluorescent behavior of nanoclusters in solution. This alteration influenced the protein's microenvironment, leading to the agglomeration of smaller monomers with other nanocluster species.

In conclusion, the implementation of a full factorial experimental design (2^2) demonstrated that the BSA/PVP interaction is statistically significant only for the 440–460 nm range, with the protein

exerting the most significant effect on fluorescence intensity. Interestingly, there was minimal variation in fluorescence intensity regardless of the quantity of polymer used.

Acknowledgment

N. Arrieta-Sandoval thanks the National Council of Science and Technology (CONACYT) for support No. 483981, in the Doctoral Program in Materials Sciences, enrolled in the National Quality Postgraduate Program (PNPC). This work was developed thanks to the financial support provided by CONACYT within the project SEP-CONACYT-CB-2016-286011.

Conflict of interest

The authors have no conflict of interest with the publication of this article.

References

1. Mathew A, Sajanlal PR, Pradeep T (2011) A fifteen atom silver cluster confined in bovine serum albumin. *J Mater Chem* 21: 11205–11212. https://doi.org/10.1039/C1JM11452B
2. Elechiguerra JL, Burt JL, Morones JR, et al. (2005) Interaction of silver nanoparticles with HIV-1. *J Nanobiotechnol* 3: 6. https://doi.org/10.1186/1477-3155-3-6
3. Kim D, Jeong S, Moon J (2006) Synthesis of silver nanoparticles using the polyol process and the influence of precursor injection. *Nanotechnology* 17: 4019–4024. https://doi.org/10.1088/0957-4484/17/16/004
4. Huang S, Christian P, Hollmann J, et al. (2012) Synthesis and characterization of colloidal fluorescent silver nanoclusters. *Langmuir* 28: 8915–8919. https://doi.org/10.1021/la300346t
5. Udayabhaskar R, Karthikeyan B, Ollakkan MS, et al. (2014) Enhanced fluorescence and optical power limiting in Ag-nanocomposite glasses. *Chem Phys Lett* 593: 1–6. https://doi.org/10.1016/j.cplett.2013.12.058
6. Verma A, Mehata MS (2016) Controllable synthesis of silver nanoparticles using Neem leaves and their antimicrobial activity. *J Radiat Res Appl Sci* 9: 109–115. https://doi.org/10.1016/j.jrras.2015.11.001
7. Kim SS, Na SI, Jo J, et al. (2008) Plasmon enhanced performance of organic solar cells using electrodeposited Ag nanoparticles. *Appl Phys Lett* 93: 305. https://doi.org/10.1063/1.2967471
8. Li B, Li J, Zhao J (2015) Silver nanoclusters emitting weak NIR fluorescence biomineralized by BSA. *Spectrochim Acta A Mol Biomol Spectrosc* 134: 40–47. https://doi.org/10.1016/j.saa.2014.06.075
9. Link S, El-Sayed MA (2000) Shape and size dependence of radiative, non-radiative and photothermal properties of gold nanocrystals. *Int Rev Phys Chem* 19: 409–453. https://doi.org/10.1080/01442350050034180
10. El-Sayed N, Schneider M (2020) Advances in biomedical and pharmaceutical applications of protein-stabilized gold nanoclusters. *J Mater Chem B* 8: 8952–8971. https://doi.org/10.1039/D0TB01610A

11. Xia H, Li F, Hu X, et al. (2016) pH-sensitive Pt nanocluster assembly overcomes cisplatin resistance and heterogeneous stemness of hepatocellular carcinoma. *ACS Cent Sci* 2: 802–811. https://doi.org/10.1021/acscentsci.6b00197
12. Biswas S, Das S, Negishi Y (2023) Advances in Cu nanocluster catalyst design: recent progress and promising applications. *Nanoscale Horiz* 8: 1509–1522. https://doi.org/10.1039/D3NH00336A
13. Chen Z, Gao L (2007) A facile and novel way for the synthesis of nearly monodisperse silver nanoparticles. *Mater Res Bull* 42: 1657–1661. https://doi.org/10.1016/j.materresbull.2006.11.028
14. Hiramatsu H, Osterloh FE (2004) A simple large-scale synthesis of nearly monodisperse gold and silver nanoparticles with adjustable sizes and with exchangeable surfactants. *Chem Mater* 16: 2509–2511. https://doi.org/10.1021/cm049532v
15. Dhanya S, Saumya V, Rao T (2013) Synthesis of silver nanoclusters, characterization and application to trace level sensing of nitrate in aqueous media. *Electrochim Acta* 102: 299–305. https://doi.org/10.1016/j.electacta.2013.04.017
16. Huang T, Murray RW (2003) Luminescence of tiopronin monolayer-protected silver clusters changes to that of gold clusters upon galvanic core metal exchange. *J Phys Chem B* 107: 7434–7440. https://doi.org/10.1021/jp0276956
17. Le Guével X, Hötzer B, Jung G, et al. (2011) Formation of fluorescent metal (Au, Ag) nanoclusters capped in bovine serum albumin followed by fluorescence and spectroscopy. *J Phys Chem C* 115: 10955–10963. https://doi.org/10.1021/jp111820b
18. Xie J, Zheng Y, Ying JY (2009) Protein-directed synthesis of highly fluorescent gold nanoclusters. *J Am Chem Soc* 131: 888–889. https://doi.org/10.1021/ja806804u
19. Pearson RG (1963) Hard and Soft Acids and Bases. *J Am Chem Soc* 85: 3533–3539, https://doi.org/10.1021/ja00905a001
20. Guo C, Irudayaraj J (2011) Fluorescent Ag clusters via a protein-directed approach as a Hg (II) ion sensor. *Anal Chem* 83: 2883–2889, 2011. https://doi.org/10.1021/ac1032403
21. Sych T, Reveguk Z, Pomogaev A, et al. (2018) Fluorescent silver clusters on protein templates: understanding their structure. *J Phys Chem C* 122: 29549–29558. https://doi.org/10.1021/acs.jpcc.8b08306
22. Bryaskova R, Pencheva D, Nikolov S, et al. (2011) Synthesis and comparative study on the antimicrobial activity of hybrid materials based on silver nanoparticles (AgNps) stabilized by polyvinylpyrrolidone (PVP). *J Chem Biol* 4: 185–191. https://doi.org/10.1007/s12154-011-0063-9
23. Kavlak S, Güner A (2006) Intermolecular interactions between bovine serum albumin and certain water-soluble polymers at various temperatures. *J Appl Polym Sci* 100: 1554–1560. https://doi.org/10.1002/app.23544
24. Dhanya S, Saumya V, Rao TP (2013) Synthesis of silver nanoclusters, characterization and application to trace level sensing of nitrate in aqueous media. *Electrochim Acta* 102: 299–305. https://doi.org/10.1016/j.electacta.2013.04.017
25. Desireddy A, Kumar S, Guo J, et al. (2013) Temporal stability of magic-number metal clusters: beyond the shell closing model. *Nanoscale* 5: 2036–2044. https://doi.org/10.1039/C3NR33705G.
26. Borsella E, Cattaruzza E, De Marchi G, et al. (1999) Synthesis of silver clusters in silica-based glasses for optoelectronics applications. *J Non-Cryst Solids* 245: 122–128. https://doi.org/10.1016/S0022-3093(98)00878-3

27. Dmitryuk AV, Paramzina SE, Perminov AS, et al. (1996) The influence of glass composition on the properties of silver-doped radiophotoluminescent phosphate glasses. *J Non-Cryst Solids* 202: 173–177. https://doi.org/10.1016/0022-3093(96)00175-5
28. Trave E, Cattaruzza E, Gonella F, et al. (2012) Ag clustering investigation in laser irradiated ion-exchanged glasses by optical and vibrational spectroscopy. *Appl Surf Sci* 258: 9399–9403. https://doi.org/10.1016/j.apsusc.2011.09.084
29. Zhao T, Sun R, Yu SH, et al. (2010) Size-controlled preparation of silver nanoparticles by a modified polyol method. *Colloids Surf A: Physicochem Eng* 366: 197–202. https://doi.org/10.1016/j.colsurfa.2010.06.005
30. Selvam S, Sundrarajan M (2012) Functionalization of cotton fabric with PVP/ZnO nanoparticles for improved reactive dyeability and antibacterial activity. *Carbohydr Polym* 87: 1419–1424. https://doi.org/10.1016/j.carbpol.2011.09.025
31. Servagent-Noinville S, Revault M, Quiquampoix H, et al. (2000) Conformational changes of bovine serum albumin induced by adsorption on different clay surfaces: FTIR analysis. *J Colloid Interface Sci* 221: 273–283. https://doi.org/10.1006/jcis.1999.6576
32. Arrondo JLR, Muga A, Castresana J, et al. (1993) Quantitative studies of the structure of proteins in solution by Fourier-transform infrared spectroscopy. *Prog Biophys Mol Biol* 59: 23–56. https://doi.org/10.1016/0079-6107(93)90006-6
33. Xing R, Guo J, Miao C, et al. (2014) Fabrication of protein-coated CdS nanocrystals via microwave-assisted hydrothermal method. *J Exp Nanosci* 9: 582–587. https://doi.org/10.1080/17458080.2012.678891
34. Csach K, JuríkováA, Miskuf J, et al. (2012) Thermogravimetric study of the decomposition of BSA-coated magnetic nanoparticles. *Acta Phys Pol A* 121: 1293–1295. https://doi.org/10.12693/APhysPolA.121.1293
35. Peniche C, Zaldívar D, Pazos M, et al. (1993) Study of the thermal degradation of poly (N-vinyl-2-pyrrolidone) by thermogravimetry–FTIR. *J Appl Polym Sci* 50: 485–493. https://doi.org/10.1002/app.1993.070500312.
36. Cedervall T, Lynch S, Berggard TE, et al. (2007) Understanding the nanoparticle-protein corona using methods to quantify exchange rates and affinities of proteins for nanoparticles. *Proc Natl Acad Sci* 104: 2050–2055. https://doi.org/10.1073/pnas.0608582104